Long-range interaction and elastic collisions of isolated vortices

TIMOUR RADKO

Department of Oceanography, Naval Postgraduate School, Monterey, CA 93943, USA
tradko@nps.edu

This study explores the interaction of two nearly axisymmetric two-dimensional vortices using a combination of numerical simulations and analytical arguments. We consider isolated or 'shielded' eddies, characterized by zero net vorticity. The ability of such vortices to propagate and interact is associated with the small dipolar component that is introduced initially. Numerical contour dynamics experiments indicate that the interaction of shielded eddies takes one of two forms, depending on their initial separation and on the relative orientation of their dipolar components. Eddies can influence each other by remotely modifying the dipolar moments of partner vortices, an effect manifested in a gentle deflection of their trajectories from a straight course. Strong interactions occur when eddies collide and rebound. The remote interaction is explained by weakly nonlinear theory in which the basic state consists of identical circularly symmetric eddies and the perturbation is assumed to be small. It is argued that the elastic rebounds observed during direct collisions are induced by the exchange of fluid between colliding vortices.

1. Introduction

The abundance of mesoscale eddies in the ocean, combined with their ability to transport mass, momentum, and energy, makes knowledge of eddy dynamics critical for understanding their role in ocean mixing. The general conclusions from all kinds of oceanographic data – see Robinson (1983) and Olson (1991) for a summary of observational results – is that eddies exist almost everywhere they have been looked for, though the distribution of eddy activity is spatially heterogeneous. The eddy field is dynamically active; mid-ocean eddies propagate large distances without loss of coherence and interact with the mean large-scale circulation and other eddies.

It has long been recognized (Adem 1956; McWilliams & Flierl 1979; Sutyrin & Flierl 1994) that the motion of intense vortices relative to the background flow is associated with the presence of a dipolar component, typically masked by the dominant axisymmetric circulation. In the ocean, this dipolar component can be produced by the action of the gradient of planetary vorticity (the so-called beta-effect), which results in the systematic westward drift of vortices (Nof 1981, 1983; Killworth 1986). However, the observed eddy propagation velocities often differ considerably, both in amplitude and direction, from that resulting from the beta-effect (e.g. Chassignet Olson & Boudra 1990). To explain the disagreement, Stern & Radko (1998) suggested that the dipolar component may also be generated or modified during the interactions of eddies with topography, other eddies, and currents. It may be produced, along with other non-axisymmetric perturbations, by the same process

that generated the eddy. The eddy translation caused by the dipolar component of non-beta origin was referred to as self-propagation. It was shown (Radko & Stern 1999, 2000) that the initially introduced dipolar component can persist for long times, dominating the beta-effect and thereby controlling the propagation characteristics. The presence of the dipolar component in two-dimensional vortices can be reflected by a small shift of the interior core relative to the vortex exterior. In stratified fluid, self-propagation can also occur if the upper part of the vortex is displaced relative to its lower part. Structures of this type are known as hetons (Hogg & Stommel 1985) and their ability to propagate and interact with other vortices has been established (Griffiths & Hopfinger 1986).

This study considers self-propagation in the context of the two-dimensional vortex–vortex interaction problem. We examine the weak, long-range interactions of separated vortices via the remotely induced velocity fields, as well as strong interactions which occur when eddies collide and exchange fluid. Both regimes are considered in terms of the eddy's ability (or inability) to resist modification of its initial dipolar component. We explain the dynamics of the vortex–vortex collisions by focusing on the time evolution of their dipolar moments, and discuss the consequences of strong and weak interaction effects for the trajectories of self-propagating vortices.

It should be mentioned that historically the vortex–vortex interactions have been discussed mostly in the framework of the classical merger problem, in which eddies are represented by finite-area patches of uniform vorticity (Christiansen & Zabusky 1973; Melander, Zabusky & McWilliams 1988; Dritschel 1986; Griffiths & Hopfinger 1987; Yasuda & Flierl 1995; among many others). These studies revealed the tendency for the two eddies to coalesce into a single vortex if their initial separation is sufficiently small. Motivated by the two-dimensional and quasi-geostrophic turbulence theories (e.g. McWilliams 1984), the merger models consider eddies with finite net vorticity and thus with finite far-field circulation. However, a more relevant model of oceanic eddies is represented by a compact structure in which the rapidly rotating core is surrounded by a compensating shield of opposite-sign vorticity (Carton 2001). The vanishing of the far-field circulation can be rationalized by energy considerations (e.g. Stern 1987). The azimuthal velocity induced by an eddy with finite net vorticity is inversely proportional to the distance from the eddy. Therefore, the kinetic energy associated with such a vortex is infinite – a significant limitation of the unshielded model in terms of its ability to represent oceanic eddies. Oceanographic measurements indicate that the typical velocity distribution of coherent vortices is rather compact and that the relative vorticity changes sign in the vortex interior (Olson 1980; Olson *et al.* 1985; Joyce & McDougall 1992; Cornillon & Park 2001). The laboratory experiments with decaying monopolar vortices also revealed a tendency for the vortices to evolve towards the shielded configuration (Trieling & van Heijst 1998; Beckers *et al.* 2001). It is the focus on the completely shielded eddies that distinguishes our study from the earlier vortex–vortex interaction models. Because of the absence of the exterior net circulation, the small initial dipolar moment becomes critical for the eddy translation and interaction with its partner. Our model is akin to the study of eddy scattering by a topographic obstacle (Stern 2000), which also emphasizes the role of the dipolar moment in the evolution of an isolated vortex.

While bringing more insight into the propagation and interaction of the oceanic eddies is our ultimate goal, it should be noted that the simplicity of our model – most notably the two-dimensional framework adopted for this study – precludes direct quantitative comparisons with oceanographic field measurements. A question often raised is whether the idealized two-dimensional models, interesting as they may be

in their own right, can provide an adequate analogue of vortices in nature. It is our belief that the proposed model will influence the interpretation of observations in two critical respects. First, it underscores the fundamental differences in the evolution of shielded and unshielded eddies, the differences which undoubtedly persist in the three-dimensional world. In addition, the techniques and ideas that we use here to derive the explicit analytical solutions are sufficiently general and could be adapted for the analysis of the interaction of various compact structures, two- or three-dimensional.

With these considerations in mind, we set out our paper as follows. In §2, we present preliminary numerical experiments with self-propagating eddies, including an example of remote interaction. The initial orientation of the eddies is such that they are able to pass each other without colliding. Still, a small but permanent deflection of the eddies from their initial course is observed and attributed to the long-range interaction. To explain its mechanics and magnitude, in §3 we develop a weakly nonlinear theory for the amplitude of the eddy dipolar component. The amplitude equations are then used to predict the vortex trajectories (§4). Section 5 addresses the dynamics of the direct collisions. We note the exchange of fluid between eddies during their brief encounter and emphasize its dynamical significance. We summarize the key findings in §6.

2. Preliminary considerations

2.1. *Formulation*

Our focus is on two-dimensional shielded eddies characterized by zero net vorticity:

$$\iint \varsigma \, \mathrm{d}x \, \mathrm{d}y = 0. \tag{1}$$

The integration in (1) is carried over a finite area (S); $\varsigma = \nabla^2 \psi$ is the vorticity, which vanishes outside the vortex, and ψ is the streamfunction. A simple model of such structures is given by a point anticyclonic vortex surrounded by a patch of uniform vorticity as shown in the schematic diagram in figure 1(*a*). The two-dimensional flow of an inviscid incompressible fluid is governed by the vorticity equation:

$$\frac{\partial \varsigma}{\partial t} + J(\psi, \varsigma) = 0, \tag{2}$$

which we cast in non-dimensional form by setting the distributed vorticity to unity and its area to π; the time variable t is non-dimensionalized accordingly: $t = t_{\mathrm{dim}} \varsigma_{\mathrm{dim}}$. In view of (1), the non-dimensional vorticity of the point vortex located at (X_0, Y_0) becomes

$$\varsigma = -\pi \delta(x - X_0) \delta(y - X_0), \tag{3}$$

where δ is the Dirac delta function.†

Motivated by observations of oceanic rings, we consider nearly axisymmetric or 'quasi-monopolar' (Stern & Radko 1998) vortices. The boundary of distributed vorticity (∂S) is only slightly perturbed relative to a unit circle, and the point vortex

---

† While the singular distribution of vorticity represents an extreme idealization, it should be mentioned that we performed a series of numerical calculations (not shown) in which a point vortex was replaced by a distributed inner core of uniform vorticity, with no circulation outside the eddy. Since the outcome of those experiments was qualitatively similar to that with singular interior vorticity, our paper will address only the more tractable singular case.
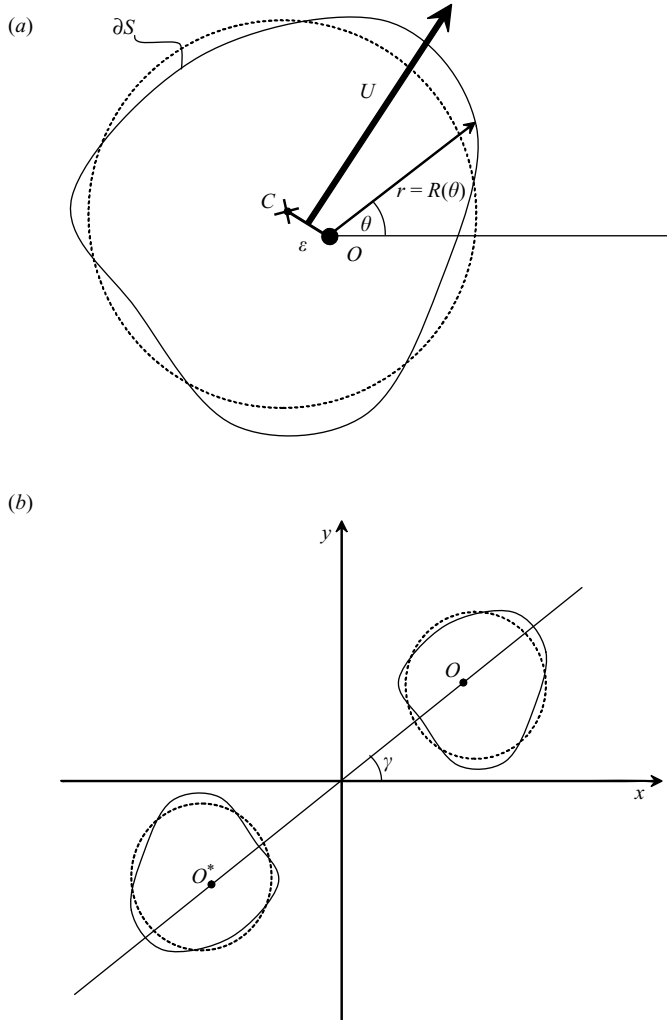
FIGURE 1. Schematic of the vorticity configurations used in our model: (*a*) One of the shielded eddies consisting of an anticyclonic point vortex (O) surrounded by a patch of uniform cyclonic vorticity. The contour of distributed vorticity (∂S) is only slightly perturbed relative to a circle (dashed) centred at C. (*b*) Two interacting eddies that are symmetric with respect to the origin of the coordinate system; O and O^* are their point vortices.

is only slightly away from its centre. The weak asymmetry is, however, dynamically significant – it causes the vortex to drift, slowly but steadily, away from its origin. The quasi-monopolar vortex in figure 1(*a*) can be viewed as a superposition of the strong circularly symmetric circulation (also known as a 'rider') and a weak dipole. Propelled by the dipolar component, partially masked by the rider, the vortex as a whole moves with the speed

$$U \approx \frac{\varepsilon}{2}, \tag{4}$$

where ε is the distance between the centroid of distributed vorticity C, marked by the plus sign in figure 1(*a*), and the point vortex O (marked by the filled circle). The

direction of motion is perpendicular to the displacement between the centroid and point vortex (e.g. Stern & Radko 1998).

An interesting feature of quasi-monopolar vortices is related to their ability to maintain speed and direction for long periods of time, resulting in propagation over distances greatly exceeding their size. The persistent character of self-propagation can be rationalized (Stern & Radko 1998) using the well-known (e.g. Saffman 1992) principle of impulse conservation, which states that, in the absence of external forcing, the dipolar moments of eddy vorticity (Q_x, Q_y) are conserved:

$$
\left.
\begin{aligned}
\frac{\mathrm{d}Q_x}{\mathrm{d}t} &= 0, \qquad Q_x = \iint x\zeta\,\mathrm{d}x\,\mathrm{d}y; \\
\frac{\mathrm{d}Q_y}{\mathrm{d}t} &= 0, \qquad Q_y = \iint y\zeta\,\mathrm{d}x\,\mathrm{d}y.
\end{aligned}
\right\}
\tag{5}
$$

For the configuration in figure 1(a), the expression for the eddy dipolar moment simplifies (Stern & Radko 1998) to

$$
(Q_x, Q_y) = \pi(X_C - X_0, Y_C - Y_0)
\tag{6}
$$

where

$$
(X_C, Y_C) = \left(\frac{1}{S} \iint_S x\,\mathrm{d}x\,\mathrm{d}y, \; \frac{1}{S} \iint_S y\,\mathrm{d}x\,\mathrm{d}y \right)
$$

are the coordinates of the centroid of the distributed vorticity patch. Equation (6) reduces to a requirement that the separation between the point vortex (X_0, Y_0) and (X_C, Y_C) does not vary in time:

$$
\frac{\mathrm{d}}{\mathrm{d}t}(X_C - X_0) = 0, \quad \frac{\mathrm{d}}{\mathrm{d}t}(Y_C - Y_0) = 0,
\tag{7}
$$

which, in turn, implies the invariance of the propagation velocity (4).

The dipolar moment can be related to the shape of the vorticity contour as follows. First, we adopt a polar coordinate system in which the origin is set at the point vortex O, and the polar axis is oriented in the x-direction (see figure 1a). In this system, the contour is described by the radius–angle relation $r = R(\theta)$, and the separation between the centroid and the point vortex becomes

$$
\left.
\begin{aligned}
X_C - X_0 &= \frac{1}{\pi} \iint_S (x - X_0)\,\mathrm{d}x\,\mathrm{d}y = \frac{1}{\pi} \int_0^{2\pi} \mathrm{d}\theta \int_0^{R(\theta)} r^2 \cos\theta\,\mathrm{d}r, \\
Y_C - Y_0 &= \frac{1}{\pi} \iint_S (y - Y_0)\,\mathrm{d}x\,\mathrm{d}y = \frac{1}{\pi} \int_0^{2\pi} \mathrm{d}\theta \int_0^{R(\theta)} r^2 \sin\theta\,\mathrm{d}r.
\end{aligned}
\right\}
\tag{8}
$$

Next, we represent the nearly circular vorticity contour in figure 1(a) in terms of its Fourier components:

$$
R(\theta) = 1 + \sum_{m=1}^{\infty} A_m \cos(m\theta) + B_m \sin(m\theta),
\tag{9}
$$

where the coefficients A_m, B_m are assumed to be small. When (9) is substituted in (8) and the result is linearized for $|A_m|, |B_m| \ll 1$, we arrive at

$$
X_C - X_0 = A_1, \quad Y_C - Y_0 = B_1.
\tag{10}
$$

Equations (10) and (6) imply that the eddy dipolar moment is proportional to the first azimuthal Fourier harmonic of the displacement of the vorticity contour relative to the point vortex.

While the conservation of the eddy dipolar moment – hence conservation of its velocity and its azimuthal $m = 1$ harmonic – controls the propagation of a single isolated vortex, the possibility exists that the dipolar moment could be substantially modified in the presence of another distant vortex. To examine the strength and typical patterns of interaction of two self-propagating vortices, their evolution is first simulated numerically. We use the contour dynamics method (Zabusky, Hughes & Roberts 1979; Stern & Pratt 1985) which makes it possible to compute the time evolution of the boundaries of uniform vorticity patches. The numerical code is similar to that in Stern & Radko (1998), but here it is applied to the two-vortex configuration shown schematically in figure 1(*b*). Each eddy is still represented by an anticyclonic point vortex surrounded by a compensating patch of uniform cyclonic vorticity. The notation adopted for the first vortex (figure 1*b*) is the same as in figure 1(*a*); the corresponding quantities for the second vortex are marked by asterisks. To reduce the number of controlling parameters, we focus here on the configurations that are symmetric which respect to the origin of the coordinate system. However, our preliminary experiments with asymmetric vortices (Appendix A) suggest that their evolutionary patterns are qualitatively similar.

2.2. *Remote interaction of isolated vortices*

The experiment in figure 2 was initialized by two vorticity contours consisting of unit circles, each represented by $N = 500$ equally spaced Lagrangian points and the compensating point vortices which were placed at

$$(X_0, Y_0) = (3, 1), \quad (X_0^*, Y_0^*) = (-3, -1). \tag{11}$$

The centres of the vorticity contours were slightly displaced with respect to (11) as follows:

$$\left.\begin{array}{l} X_C = X_0, \ Y_C = Y_0 - 0.05, \\ X_C^* = X_0^*, \ Y_C^* = Y_0^* + 0.05. \end{array}\right\} \tag{12}$$

As discussed earlier – see (4) – this small *y*-displacement introduces a dipolar moment which propels vortices in the *x*-direction. The initial configuration in (11) and (12) is such that the vortices are able to pass each other without collision, which we refer to as the weak interaction regime.

The first stage of the numerical experiment (figure 2*a*) represents the rectilinear motion of vortices – so far, the vortices exert only a slight influence on their partners and the trajectories are almost straight. This pattern of motion, however, changes when eddies come into close proximity (figure 2*b*, *c*). Their trajectories become visibly deflected: first, the eddies make a gentle right turn (figure 2*b*) and then, after passing their partner, turn left (figure 2*c*). The vortices do not recover their initial orientation, and the net effect of their weak encounter is to produce a finite *y*-velocity component – the component which was absent initially. As a result, the vortices scatter at a finite angle relative to their original direction of motion. The change in propagation velocity also implies that the eddy dipolar moment has also been permanently modified.

The strength of the remote interaction of isolated vortices can be roughly estimated by the following scaling analysis. The far-field advection induced by a circular patch of unit vorticity with area π is represented by a streamfunction:

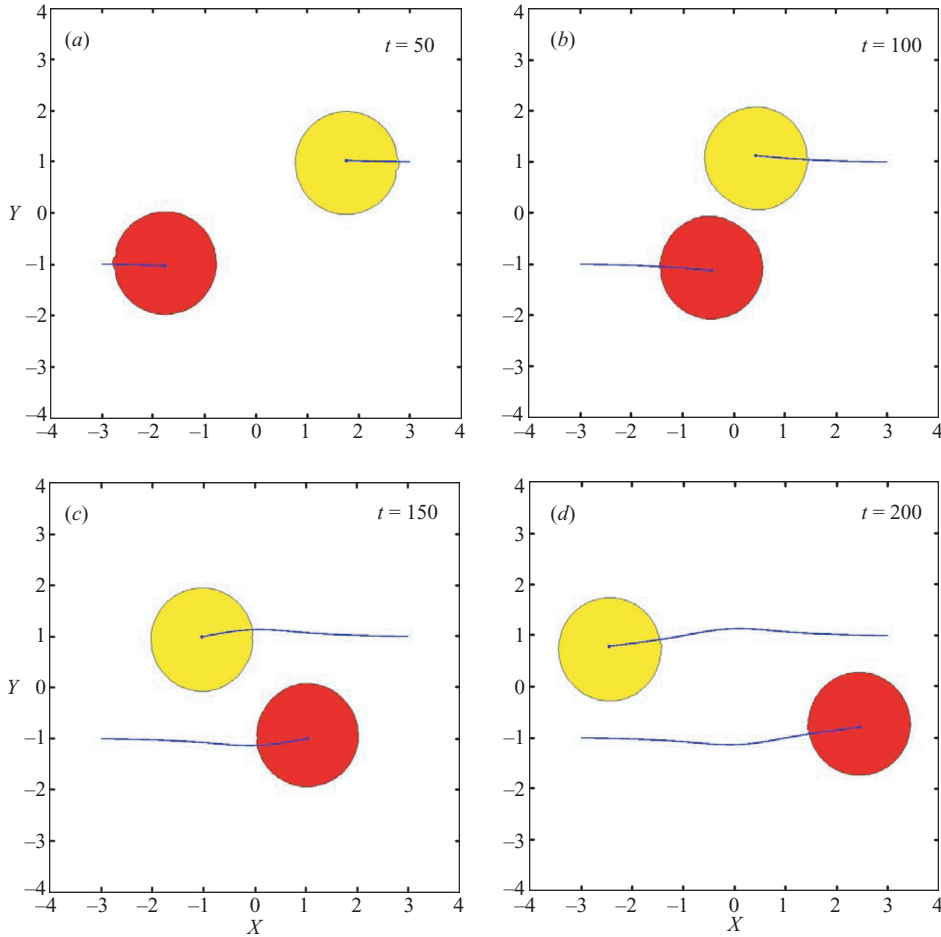$$\psi_C = \tfrac{1}{4}\ln((x - X_C)^2 + (y - Y_C)^2), \tag{13}$$

FIGURE 2. Numerical experiment with non-colliding vortices. The regions of distributed vorticity are shown in red and yellow, and the blue curves represent trajectories of the point vortices. Note the small but permanent change in the direction of motion caused by the remote interaction of eddies.

and the streamfunction of the point vortex is

$$\psi_0 = -\tfrac{1}{4}\ln((x - X_0)^2 + (y - Y_0)^2). \tag{14}$$

The sum of (13) and (14) reduces, for $|X_0 - X_C|, |Y_0 - Y_C| \sim \varepsilon \ll 1$, to

$$\psi \approx \frac{1}{2}\frac{(x - X_C)(X_0 - X_C) + (y - Y_C)(Y_0 - Y_C)}{(x - X_C)^2 + (y - Y_C)^2}. \tag{15}$$

Thus, the velocity induced by the vortex on its partner is relatively weak:

$$\psi \sim \frac{\varepsilon}{l}; \ (u, v) = \left(-\frac{\partial \psi}{\partial y}, \frac{\partial \psi}{\partial x}\right) \sim \frac{\varepsilon}{l^2}, \tag{16}$$

where l is the distance between the two vortices. This velocity is also non-uniform. For instance, the difference between the velocity of the second point vortex (O^*) and

the velocity of particles located at the centroid of the second vortex (C^*) is

$$\left.\begin{array}{l} \Delta u = u_C^* - u_0^* \approx \nabla u \cdot (X_C^* - X_0^*, Y_C^* - Y_0^*) \sim \dfrac{\varepsilon^2}{l^3}, \\[2mm] \Delta v = v_C^* - v_0^* \approx \nabla v \cdot (X_C^* - X_0^*, Y_C^* - Y_0^*) \sim \dfrac{\varepsilon^2}{l^3}. \end{array}\right\} \tag{17}$$

This non-uniformity of the induced velocity field implies that the eddy dipolar moment – the eddy's 'engine' responsible for its propagation – can change in time at the rate of

$$\frac{\partial}{\partial t}(X_C^* - X_0^*) \sim \frac{\partial}{\partial t}(Y_C^* - Y_0^*) \sim \frac{\varepsilon^2}{l^3}. \tag{18}$$

Since the dipolar moment of quasi-monopolar vortices is small ($\varepsilon \ll 1$), whereas the separation between the eddies should at least exceed their diameter ($l > 2$), the estimate in (18) explains why the interaction of vortices in figure 2 is rather weak and why significant effects occur only when vortices are close to each other.

Of course, the foregoing crude estimate oversimplifies the dynamics of interaction. Vorticity contours are not exactly circular and, more importantly, the velocity of the centroid may differ considerably from the Lagrangian particle velocities at the same location. Nevertheless, the subsequent formal asymptotic analysis (§ 3) confirms the anticipated scaling in (18).

2.3. *Head-on collision of self-propagating vortices*

Figure 3 presents an example of the direct collision of self-propagating eddies. The point vortices were placed at

$$(X_0, Y_0) = (3, 0), \quad (X_0^*, Y_0^*) = (-3, 0) \tag{19}$$

and the displacement of the distributed vorticity centres was the same as in our previous experiment (12). This configuration corresponds to the motion of eddies along the x-axis directly towards each other. Figure 3(a, b) reveals that initially eddies move in a remarkably straight path. The magnitude of propagation velocity is also almost uniform in time. As vortices approach their partner they tend to accelerate slightly until their head-on collision (figure 3c). It should be noted that the collision involves a considerable exchange of fluid: part of the first vortex (yellow patch in figure 3c) leaks into the second vortex (red patch) and vice versa. After the collision, vortices rebound, rapidly reversing their course (figure 3d), and then steadily drift away from each other. A thin vorticity filament connecting the two vortices in figure 3(d) is the only reminder of their violent encounter.

The observed rebound is almost elastic in the sense that the vortex speed before the collision is close to its speed after. It is only the direction of motion that changes dramatically. Reversal of the course implies that the eddy dipolar moment has also been reversed. Consider, say, the yellow eddy in figure 3. Before the collision, the eddy centroid was located below the point vortex – 'below' refers here to the negative y-direction – and the eddy drifted in the negative x-direction. After collision, the eddy started to translate in the positive x-direction, which implies that the centroid has moved above the point vortex. This displacement of the centroid relative to the point vortex can be readily attributed to the exchange of fluid between the two eddies. During the encounter, the first eddy loses some fluid in its lower (negative-y) part, which is compensated by the entrainment of fluid from the second vortex into its upper part. Such an exchange, clearly visible in figure 3(c), effectively displaces the
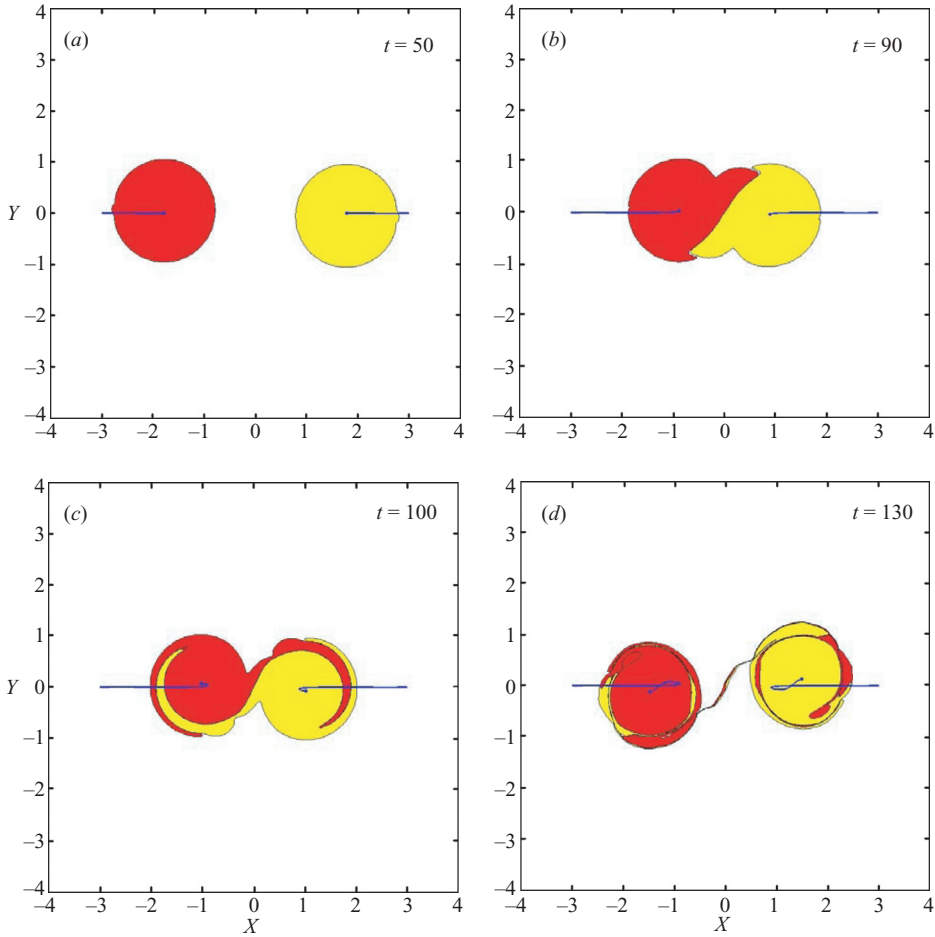
FIGURE 3. The same as in figure 2 but for colliding vortices. Note the substantial exchange of fluid between eddies during the collision.

centroid of distributed vorticity in the positive y-direction, thereby reversing the eddy dipolar moment and, eventually, its direction of motion.

In the following section, we quantify and extend our physical interpretation of eddy–eddy interactions by developing a formal asymptotic theory in which ε – the measure of eddy dipolar moment – is small.

3. Weakly nonlinear theory for the vortex–vortex interaction

Motivated by the numerical simulations in §2, we attempt to describe the dynamics of the interacting eddies analytically, by predicting the evolution of their dipolar moments. Without loss of generality, we temporarily adopt the coordinate system shown schematically in figure 4, in which the first point vortex (O) is located at the origin (i.e. $(X_0, Y_0) = (0, 0)$) and the second point vortex (O^*) is located on the x-axis ($(X_0^*, Y_0^*) = (-l, 0)$). This coordinate system is stationary in the sense that it does not follow the moving vortex – vortices are aligned along the x-axis only at given instant of time.
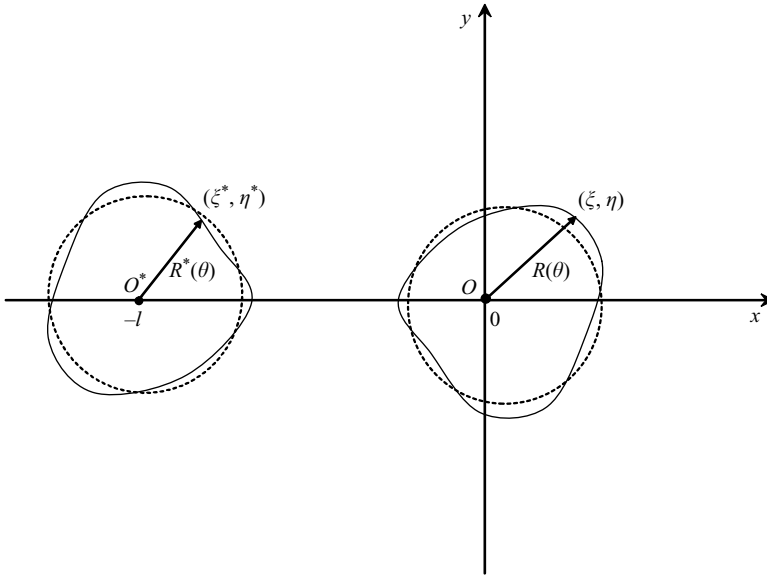
FIGURE 4. The coordinate system used in formulating the weakly nonlinear model. Its origin is placed at the instantaneous location of the first point vortex (O) and the x-axis is oriented along the line (O^*, O) connecting the point vortices. (ξ, η) represent the Cartesian coordinates of the points located on the vorticity contour of the first eddy; (ξ^*, η^*) are the coordinates of the second.

3.1. *Governing equations*

The first vorticity contour (ξ, η) can be described in polar coordinates (r, θ) such that:

$$r = R(\theta) = \sqrt{\xi^2 + \eta^2}, \quad \cos\theta = \frac{\xi}{r}, \quad \sin\theta = \frac{\eta}{r}, \tag{20}$$

and the second vorticity contour (ξ^*, η^*) can be represented similarly (see the schematic in figure 4):

$$r = R^*(\theta) = \sqrt{(\xi^* + l)^2 + (\eta^*)^2}, \quad \cos\theta = \frac{\xi^* + l}{r}, \quad \sin\theta = \frac{\eta^*}{r}. \tag{21}$$

Since we restricted our discussion to configurations in which two eddies are perfectly symmetric with respect to each other, we write this condition in polar coordinates as follows

$$R^*(\theta) = R(\theta + \pi). \tag{22}$$

If satisfied initially, (22) holds at all times.

The evolution of the contour $r = R(\theta)$ in time is computed as follows. Let $\boldsymbol{n}$ denote the outward unit vector normal to the interface and $\boldsymbol{V}(\theta) = (U, V)$ is the velocity of particles at the boundary of the distributed vorticity patch relative to the point vortex. Since this boundary represents a material surface – particles initially located at this surface remain there forever – its advancement in the direction normal to the interface is exactly equal to the $\boldsymbol{n}$-projection of particle velocities:

$$\left(\frac{\mathrm{d}(x - X_0)}{\mathrm{d}t}, \frac{\mathrm{d}(y - Y_0)}{\mathrm{d}t} \right) \cdot \boldsymbol{n} = \boldsymbol{V} \cdot \boldsymbol{n}. \tag{23}$$

Returning to the polar coordinate system, we write the kinematic boundary condition (23) in terms of the evolutionary equation for R:

$$\frac{\partial R}{\partial t}\bigg|_{\theta} = \frac{V \cdot n}{n_x \cos\theta + n_y \sin\theta}. \tag{24}$$

The normal n in (24) can be readily computed from an expression for the vorticity contour $r = R(\theta)$ and the assumed symmetry condition (22) spares us from considering the evolution of the second contour, which simplifies the analysis.

Next, V in (24) is written as the difference between the velocity of particles located at the contour (V_C) and the velocity of the point vortex (V_0):

$$V = V_C - V_0. \tag{25}$$

V_C and V_0, in turn, can be separated into the distinct dynamic components:

$$V_C = V_{CC} + V_{0C} + V_{CC}^* + V_{0C}^*, \tag{26}$$

where V_{CC}, V_{0C}, V_{CC}^*, and V_{0C}^* represent the advection of the contour induced by the first distributed vortex, first point vortex, second distributed vortex, and the second point vortex respectively; and

$$V_0 = V_{C0} + V_{C0}^* + V_{00}^*, \tag{27}$$

where V_{C0}, V_{C0}^*, and V_{00}^* represent the advection of the first point vortex by the first distributed vortex, second distributed vortex, and second point vortex respectively.

The influence of distributed vortices can be described by the well-known (Zabusky *et al.* 1979) contour dynamics equations

$$\left. \begin{aligned} u &= -\frac{\varsigma}{4\pi} \oint \mathrm{d}\xi \, \ln((x-\xi)^2 + (y-\eta)^2), \\ v &= -\frac{\varsigma}{4\pi} \oint \mathrm{d}\eta \, \ln((x-\xi)^2 + (y-\eta)^2), \end{aligned} \right\} \tag{28}$$

which express the velocity (u, v) induced at a point (x, y) by a patch of uniform vorticity ($\varsigma = 1$ in our case) as the line integral along its boundary (ξ, η). Applying these equations to the first distributed vortex and returning to the polar coordinate system, we express $V_{CC} = (U_{CC}, V_{CC})$ in (26) as follows:

$$\left. \begin{aligned} U_{CC} &= -\frac{1}{4\pi} \int_0^{2\pi} \ln([R(\theta)\cos\theta - R(\varphi)\cos\varphi]^2 \\ &\quad + [R(\theta)\sin\theta - R(\varphi)\sin\varphi]^2) \frac{\mathrm{d}[R(\varphi)\cos\varphi]}{\mathrm{d}\varphi} \, \mathrm{d}\varphi, \\ V_{CC} &= -\frac{1}{4\pi} \int_0^{2\pi} \ln([R(\theta)\cos\theta - R(\varphi)\cos\varphi]^2 \\ &\quad + [R(\theta)\sin\theta - R(\varphi)\sin\varphi]^2) \frac{\mathrm{d}[R(\varphi)\sin\varphi]}{\mathrm{d}\varphi} \, \mathrm{d}\varphi, \end{aligned} \right\} \tag{29}$$

and analogous integral expressions are obtained for $V_{CC}^* = (U_{CC}^*, V_{CC}^*)$, $V_{C0} = (U_{C0}, V_{C0})$, and $V_{C0} = (U_{C0}, V_{C0})$.

Point vortices with circulation $-\pi$ produce axisymmetric streamfunctions $\psi_0 = -\frac{1}{4}\ln(x^2+y^2)$ and $\psi_0^* = -\frac{1}{4}\ln((x+l)^2+y^2)$, and the corresponding velocity components

advecting the first and second contours are

$$
\left.\begin{aligned}
U_{0C} &= \frac{1}{2}\frac{R\sin\theta}{(R\cos\theta)^2 + (R\sin\theta)^2}, & V_{0C} &= -\frac{1}{2}\frac{R\cos\theta}{(R\cos\theta)^2 + (R\sin\theta)^2}, \\
U_{0C}^* &= \frac{1}{2}\frac{R\sin\theta}{(R\cos\theta + l)^2 + (R\sin\theta)^2}, & V_{0C}^* &= -\frac{1}{2}\frac{R\cos\theta + l}{(R\cos\theta + l)^2 + (R\sin\theta)^2}.
\end{aligned}\right\} \tag{30}
$$

Finally, advection of the first point vortex by the second one is just $(U_{00}^*, V_{00}^*) = (0, -1/2l)$.

3.2. *Asymptotic expansion*

The solution of governing equations (24)–(30) proceeds by way of asymptotic expansions. To describe the interaction of two almost circular vortices analytically, we construct the power series

$$
\left.\begin{aligned}
R(\theta) &= 1 + \varepsilon\Delta R_1(\theta) + \varepsilon^2\Delta R_2(\theta) + O(\varepsilon^3) \\
R^*(\theta) &= 1 + \varepsilon\Delta R_1^*(\theta) + \varepsilon^2\Delta R_2^*(\theta) + O(\varepsilon^3),
\end{aligned}\right\} \tag{31}
$$

where ε is a small parameter measuring the displacement of the point vortex relative to the centroid of distributed vorticity. Based on the scaling arguments in §2 – see (18) – we expect the vortex–vortex interaction to affect their propagation characteristics on a relatively slow time scale $\sim\varepsilon^{-1}$, and therefore the time variable is rescaled as

$$
t = \varepsilon^{-1}t_0. \tag{32}
$$

On this time scale, our evolutionary equation (24) becomes

$$
\varepsilon\frac{\partial R}{\partial t_0} = \frac{\boldsymbol{V}\cdot\boldsymbol{n}}{n_x\cos\theta + n_y\sin\theta}. \tag{33}
$$

Our goal is to predict the evolution of the $m = 1$ azimuthal mode, primarily responsible for the propagation of isolated eddies. Therefore, at first one might be tempted to search for a solution whose first-order component consists entirely of the first harmonic. However, in the two-vortex configuration, such a solution cannot be valid over long (order ε^{-1}) time scales: as we demonstrate in Appendix B, vortex–vortex interaction causes a linear response to the $m = 1$ mode in terms of the $m = 2$ harmonic which develops at the fast ($\Delta t \sim 1$) time scale. Therefore, at this order, we also include the $m = 2$ mode whose amplitude is such that a balanced solution, evolving on the slow time scale, could be found:

$$
\Delta R_1 = A_{11}\cos\theta + B_{11}\sin\theta + A_{12}\cos(2\theta) + B_{12}\sin(2\theta). \tag{34}
$$

In view of the symmetry relation (22), the first-order structure of the second contour is given by

$$
\Delta R_1^* = -A_{11}\cos\theta - B_{11}\sin\theta + A_{12}\cos(2\theta) + B_{12}\sin(2\theta). \tag{35}
$$

The nonlinear interaction of terms in (34) and (35) is expected to produce the azimuthal harmonics 0–4, and thus we further expand our solution to the next

$(O(\varepsilon^2))$ order as follows:

$$
\left.
\begin{aligned}
R(\theta) &= 1 + \varepsilon \left[\sum_{m=1}^{2} (A_{1m} \cos(m\theta) + B_{1m} \sin(m\theta)) \right] \\
&\quad + \varepsilon^2 \left[C + \sum_{m=1}^{4} (A_{2m} \cos(m\theta) + B_{2m} \sin(m\theta)) \right] + O(\varepsilon^3), \\
R^*(\theta) &= 1 + \varepsilon \left[\sum_{m=1}^{2} (-1)^m (A_{1m} \cos(m\theta) + B_{1m} \sin(m\theta)) \right] \\
&\quad + \varepsilon^2 \left[C + \sum_{m=1}^{4} (-1)^m (A_{2m} \cos(m\theta) + B_{2m} \sin(m\theta)) \right] + O(\varepsilon^3).
\end{aligned}
\right\}
\tag{36}
$$

3.3. *The amplitude equation*

The following is an outline of the derivation of the closed system of amplitude equations for the $m = 1$ mode ($A_{11}(t_0)$ and $B_{11}(t_0)$ terms). First, the power series (36) are substituted in the expressions for the individual velocity components ($V_{CC}, V_{0C}, V_{CC}^*, V_{0C}^*, V_{C0}, V_{C0}^*, V_{00}^*$), which are then combined using (25)–(27) and substituted in the evolutionary equation (33). Next, we collect the terms of the same order in ε. The zero-order terms represent our basic state – a trivial steady configuration consisting of two non-interacting axisymmetric vortices. Combining the linear (order-ε) terms, we express the $m = 2$ components A_{12} and B_{12} in terms of (A_{11}, B_{11}). At $O(\varepsilon^2)$, it is possible to eliminate the second-order quantities (A_{2m}, B_{2m}) in favour of the first-order terms and thereby derive a solvability condition for the slow evolution of the $m = 1$ mode.

The procedure summarized above involves extensive, although fairly straightforward, algebra and therefore many details are omitted. It is perhaps worth mentioning a few standard methods used to compute the contour dynamics integrals (e.g. (29)). (i) Integrals involving the logarithm of periodic functions were simplified by integrating by parts

$$
\int_0^{2\pi} \ln(G(\varphi)) f(\varphi) \, P \mathrm{d}\varphi = - \int_0^{2\pi} \frac{G'(\varphi)}{G(\varphi)} F(\varphi) \, \mathrm{d}\varphi,
$$

where $F(\varphi) = \int f(\varphi) \, \mathrm{d}\varphi$. (ii) To integrate a combination of trigonometric functions over the interval $0 < \varphi < 2\pi$, we apply the variable change $z = \exp(\mathrm{i}\varphi)$, which transforms the integration path to the unit circle in the complex plane. Those integrals are evaluated using the residue theorem $\int g(z) \, \mathrm{d}z = 2\pi \mathrm{i} \sum \mathrm{Res}(a_k)$, where a_k are the poles of $g(z)$. (iii) Finally, at each order in ε, we simplify the formulation by considering the long-range limit $l \to \infty$. Since our estimates in §2 indicate that the strength of the vortex–vortex interaction is $\sim l^{-3}$, we expand our balanced equations in powers of l^{-1}, truncating the expansion at the third order.

In particular, the $O(\varepsilon)$ velocity components (equations (25)–(27)) represent the following linear combination of the first-order terms (A_{1i}, B_{1i}):

$$
U_{01} = \frac{1}{2l^3}(-B_{11}l + B_{12} + B_{11}l^3), \quad V_{01} = -\frac{1}{2l^3}(A_{11}l - A_{12} + A_{11}l^3) \, .
\tag{37}
$$

Here, (U_{01}, V_{01}) denote the first-order terms in the ε-expansion of the velocity of the point vortex:

$$
U_0 = U_{01}\varepsilon + U_{02}\varepsilon^2 + O(\varepsilon^3), \quad V_0 = V_{01}\varepsilon + V_{02}\varepsilon^2 + O(\varepsilon^3).
\tag{38}
$$

For the vorticity contours, we obtain

$$
\begin{aligned}
U_1 &= \frac{1}{2l^3}(B_{11}\cos(2\theta)l^3 - A_{12}\sin(3\theta)l^3 + B_{12}\cos(3\theta)l^3 - A_{11}\sin(2\theta)l^3 \\
&\quad - B_{11}l^3 + 2B_{11}\cos(\theta) + 2A_{11}\sin(\theta)), \\
V_1 &= \frac{1}{2l^3}(-2B_{11}\sin(\theta) + 2A_{11}\cos(\theta) + A_{11}\cos(2\theta)l^3 + B_{11}\sin(2\theta)l^3 \\
&\quad + B_{12}\sin(3\theta)l^3 + A_{11}l^3 + A_{12}\cos(3\theta)l^3),
\end{aligned} \right\} \tag{39}
$$

where (U_1, V_1) denote the first-order terms in the ε-expansion of the velocity of the interface relative to the point vortex:

$$
U = U_1\varepsilon + U_2\varepsilon^2 + O(\varepsilon^3), \quad V = V_1\varepsilon + V_2\varepsilon^2 + O(\varepsilon^3). \tag{40}
$$

When (39) and (40) are substituted in the evolutionary equation (33), we obtain the following order-ε balance:

$$
-\tfrac{1}{2}A_{12}l^3\sin(2\theta) + \tfrac{1}{2}B_{12}l^3\cos(2\theta) + B_{11}\cos(2\theta) + A_{11}\sin(2\theta) = 0. \tag{41}
$$

We emphasize that the linear balance (41) does not contain time derivatives which, in view of (32), enter at the next order. Equation (41) also does not contain the $m = 1$ terms. As one could have expected from the scaling analysis in §2, development of the dipolar moment via vortex–vortex interaction is indeed a fundamentally nonlinear process. Isolating the terms proportional to $\sin(2\theta)$ and $\cos(2\theta)$ in (41), we determine the $O(\varepsilon)$ components of the $m = 2$ harmonic:

$$
A_{12} = \frac{2A_{11}}{l^3}, \quad B_{12} = -\frac{2B_{11}}{l^3}, \tag{42}
$$

which implies that the $m = 2$ mode is much weaker than the $m = 1$ mode and has only an $O(l^{-6})$ effect on the point vortex velocity (37). Neglecting the corresponding $O(l^{-6})$ terms in (37) reduces it to

$$
U_{01} = \frac{-B_{11} + B_{11}l^2}{2l^2}, \quad V_{01} = -\frac{A_{11} + A_{11}l^2}{2l^2}. \tag{43}
$$

The $O(\varepsilon^2)$ balances yield the following second-order velocity components:

$$
\begin{aligned}
U_2 &= \frac{1}{8}\left(4A_{11}^2\sin\theta + 4B_{11}^2\sin\theta + A_{11}^2\sin(3\theta) - B_{11}^2\sin(3\theta) - 2B_{11}A_{11}\cos(3\theta)\right) \\
&\quad + \frac{1}{8L^3}\left(-4B_{11}A_{11} + 2\sin(4\theta)A_{11}^2 + 4A_{11}^2\sin(2\theta)\right. \\
&\quad + 2B_{11}^2\sin(4\theta) + 4B_{11}A_{11}\cos(2\theta)) + L_U(\Delta R_2), \\
V_2 &= \frac{1}{8}\left(-4B_{11}^2\cos\theta + B_{11}^2\cos(3\theta) - A_{11}^2\cos(3\theta) - 4A_{11}^2\cos\theta - 2B_{11}A_{11}\sin(3\theta)\right) \\
&\quad + \frac{1}{8L^3}\left(8B_{11}A_{11}\sin(2\theta) - 4A_{11}^2 + 4B_{11}^2 - 4B_{11}^2\cos(4\theta) - 4A_{11}^2\cos(4\theta)\right. \\
&\quad + 8B_{11}^2\cos(2\theta)) + L_V(\Delta R_2),
\end{aligned} \right\}
$$

$$
\tag{44}
$$

where L_U and L_V are the linear operators in the velocity equations (written explicitly in (B4), (B5)) acting here on the second-order terms in the expansion of R.

Substituing (44) and (40) in the evolutionary equation (33), we arrive at the following order-ε^2 balance:

$$\frac{\partial A_{11}}{\partial t_0} \cos\theta + \frac{\partial B_{11}}{\partial t_0} \sin\theta + \frac{\partial A_{12}}{\partial t_0} \cos(2\theta) + \frac{\partial B_{12}}{\partial t_0} \sin(2\theta)$$

$$= \frac{1}{8l^3} \big(32 A_{11}^2 \sin(3\theta) + 32 B_{11}^2 \sin(3\theta) + 16 A_{11} B_{11} \cos\theta - 10 A_{11} B_{11} l^3 \cos(2\theta)$$

$$- 5 B_{11}^2 \sin(2\theta) - 8 B_{11}^2 \sin\theta + 8 A_{11}^2 \sin\theta + 5 A_{11}^2 l^3 \sin(2\theta) \big) + L_R(\Delta R_2), \quad (45)$$

where $L_R = L_U \cos\theta + L_V \sin\theta$ (as previously, we consider the long-range $l \to \infty$ limit and discard the $o(l^{-3})$ terms). Since the linear operator L_R does not produce the $m = 1$ harmonic (see (41) or (B6) in Appendix B), we obtain a closed system of equations for the first-order quantities simply by isolating terms proportional to $\sin\theta$ and $\cos\theta$ in (45):

$$\frac{\partial A_{11}}{\partial t_0} = \frac{2 A_{11} B_{11}}{l^3}, \quad \frac{\partial B_{11}}{\partial t_0} = \frac{A_{11}^2 - B_{11}^2}{l^3}. \quad (46)$$

These are the amplitude equations sought for the dipolar moment. As expected (see (18)), they are characterized by quadratic nonlinearity and the strength of vortex–vortex interaction is inversely proportional to third power of the separation between vortices. When written in terms of un-rescaled quantities ($A = \varepsilon A_{11}$, $B = \varepsilon B_{11}$, and $t = \varepsilon^{-1} t_0$), the amplitude equations become

$$\frac{\partial A}{\partial t} = \frac{2AB}{l^3}, \quad \frac{\partial B}{\partial t} = \frac{A^2 - B^2}{l^3}. \quad (47)$$

4. Trajectories of interacting vortices

In this section, the amplitude equations (47) are used to predict trajectories of interacting vortices. Since we are now concerned with the finite displacements of vortices, we can no longer use a coordinate system where vortices are located on the x-axis. Therefore, we return to the coordinate system in figure 1(b); this transformation is executed by replacing the variables in (43) and (47) as follows:

$$\left. \begin{array}{l} A \to A \cos\gamma + B \sin\gamma, \quad B \to -A \sin\gamma + B \cos\gamma, \\ U_0 \to U_0 \cos\gamma + V_0 \sin\gamma, \quad U_0 \to -U_0 \sin\gamma + V_0 \cos\gamma, \end{array} \right\} \quad (48)$$

where γ is the inclination of the line (O^*, O) connecting the point vortices relative to the x-axis.

The amplitude equations become:

$$\left. \begin{array}{l} \dfrac{\partial A}{\partial t} = \dfrac{B^2 \sin(3\gamma) - A^2 \sin(3\gamma) + 2AB \cos(3\gamma)}{l^3}, \\[2mm] \dfrac{\partial B}{\partial t} = \dfrac{2AB \sin(3\gamma) - B^2 \cos(3\gamma) + A^2 \cos(3\gamma)}{l^3}, \end{array} \right\} \quad (49)$$

and the velocity of the point vortex (43) becomes:

$$\left. \begin{array}{l} U_0 = \dfrac{A \sin(2\gamma) - B \cos(2\gamma) + Bl^2}{2l^2}, \\[2mm] V_0 = -\dfrac{B \sin(2\gamma) + A \cos(2\gamma) + Al^2}{2l^2}. \end{array} \right\} \quad (50)$$

Note that (50) represents the leading-order components of the propagation velocity, and the relative error of this approximation, due to the neglect of higher-order terms in the ε-expansion, is $O(\varepsilon)$.

Next, we denote the Cartesian coordinates of the first point vortex by $X_0(t)$ and $Y_0(t)$; the coordinates of the second become $(X_0^*, Y_0^*) = (-X_0, -Y_0)$, $l = 2\sqrt{X_0^2 + Y_0^2}$, and

$$X_0 = \frac{l}{2}\cos\gamma, \quad Y_0 = \frac{l}{2}\sin\gamma. \tag{51}$$

Combining (49)–(51), we arrive at a closed system of ordinary differential equations:

$$
\left.
\begin{aligned}
\frac{\partial A}{\partial t} &= \frac{B^2 \sin(3\gamma) - A^2 \sin(3\gamma) + 2AB\cos(3\gamma)}{l^3}, \\
\frac{\partial B}{\partial t} &= \frac{2AB\sin(3\gamma) - B^2\cos(3\gamma) + A^2\cos(3\gamma)}{l^3}, \\
\frac{\partial X_0}{\partial t} &= \frac{A\sin(2\gamma) - B\cos(2\gamma) + Bl^2}{2l^2}, \\
\frac{\partial Y_0}{\partial t} &= -\frac{B\sin(2\gamma) + A\cos(2\gamma) + Al^2}{2l^2},
\end{aligned}
\right\} \quad l = 2\sqrt{X_0^2 + Y_0^2}, \ \gamma = \arg(X_0 + iY_0),
\tag{52}
$$

which can be solved for any given initial conditions for (X_0, Y_0, A, B). However, before presenting specific solutions, we note that the system (52) is invariant under the transformation

$$
\left.
\begin{aligned}
(X, Y) &\to (X, Y), \\
(A, B) &\to M_0^{-1}(A, B), \\
t &\to M_0 t,
\end{aligned}
\right\}
\tag{53}
$$

where M_0 is an arbitrary constant. Choosing $M_0 = \sqrt{A(0)^2 + B(0)^2}$, we can, without loss of generality, consider only the reference case with unit initial amplitude of the $m = 1$ mode ($\sqrt{A(0)^2 + B(0)^2}$) and just examine various initial orientations of vortices. As (53) indicates, variation of the initial amplitude of the dipolar component does not affect the trajectory, and the propagation time can be recovered by dividing t in the reference experiment by M_0. Also without loss of generality, we assume that the eddy dipolar component is initially oriented in the y-direction, i.e. $A(0) = 0$. Thus, the parameter space of initial conditions is effectively described by just two variables $[X_0(0), Y_0(0)]$ representing the initial location of the first vortex.

Figure 5 presents a set of trajectories computed with $X_0(0) = 3$ and various values of $Y_0(0)$. Calculations were terminated when the separation between the vortices reduced to $l = 2$, as it was assumed that at that moment vortices collided. Trajectories in figure 5 reflect the major features of the fully nonlinear numerical experiments (§2). If the initial offset in y between eddies is small, $|Y_0| < 0.87$, the eddies collide as in figure 3. However if $|Y_0| > 0.87$, vortices are able to pass each other and their pattern of motion is similar to that in figure 2. At first, eddies are largely unaffected by their partners: propelled by the initially introduced dipolar moment, they move in a straight path. As eddies come closer, they deflect from their initial course, first slightly away from the x-axis – to avoid the approaching partner – and then towards the x-axis. Overall, the remote interaction of eddies results in a small but permanent change in their direction of motion.

Figure 6 presents a comparison of the asymptotic theory and numerical simulations. In figure 6(a, b), we superimpose the records of $X_0(t)$ and $Y_0(t)$ from the contour
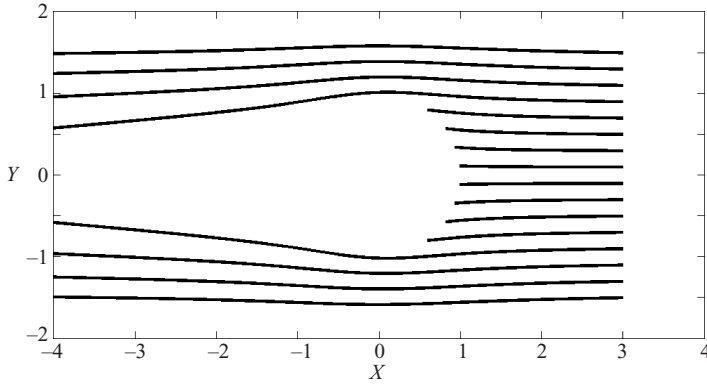
FIGURE 5. Trajectories predicted by the theoretical model for one of the interacting eddies. Note the small but permanent change in the direction of motion.
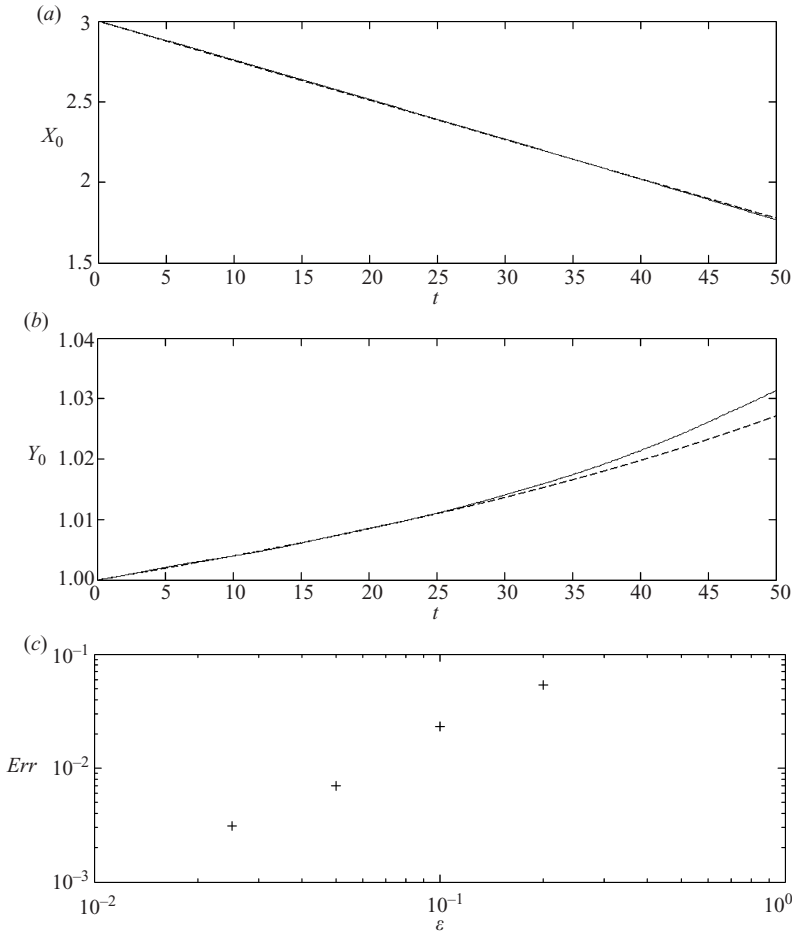

FIGURE 6. Comparison of the numerical calculation with the asymptotic theory: (*a*) *x*-coordinate of the point vortex *O* as a function of time from the numerical experiment in figure 2 (solid curve) and from the theoretical model (dashed curve); (*b*) *y*-coordinate for the same experiment; (*c*) the error of the asymptotic theory, relative to the contour dynamics experiment, as a function of ε.

dynamical experiment in figure 2 (solid curve) with the corresponding theoretical prediction (dashed curve). To be consistent with the long-range ($l \gg 1$) assumption of the asymptotic model, we present an early stage of the experiment ($0 < t < 50$) when eddies are still significantly separated from each other. The general agreement between the numerics and theory supports the proposed weakly nonlinear model of the remote eddy–eddy interaction. A more quantitative test of the asymptotic theory is presented in figure 6(c). We performed a series of contour dynamical experiments with $\varepsilon = 0.025$, 0.05, 0.1, and 0.2, whereas other parameters were the same as in figure 2. In each experiment, we recorded the separation distance of the point vortex from its origin for one rescaled unit of time ($t_0 = 1$), which corresponds to $t = \varepsilon^{-1}$. The difference between the numerical and theoretical separation (*Err*) is plotted as a function of ε in logarithmic coordinates. As expected, the relative error in figure 6(c) is proportional to ε.

5. Elastic collisions of isolated eddies

In this section, we explore dynamics of the direct vortex–vortex collisions, such as shown in figure 3. After brief collisions, eddies rebound and move away, dramatically changing their direction of motion and thus their dipolar moments. How is this possible? Our theoretical considerations (figure 5), as well as experiments with non-colliding eddies (figure 2) indicate that the dipolar moment is a fairly robust quantity and cannot be easily modified, much less reversed. Even when eddies just nearly miss each other, the variation in their dipolar moment does not exceed 15 %.

We believe that a fundamental distinction between the dynamics of colliding and nearly colliding cases is related to the exchange of fluid between vortices during their direct contact. It was proposed in §2 that such an exchange provides an efficient mechanism for modification of the eddy dipolar moment. As illustrated in figure 3(c), entrainment of fluid on one side of the vortex from its partner, combined with the equivalent loss of fluid at the opposite side, effectively displaces the centroid by an amount (Δ) proportional to the area (S_{ex}) of the entrained fluid. This displacement modifies the separation between the centroid and the point vortex which is, in turn, proportional to the propagation velocity. The proposed scenario leads us to a simple testable prediction of the magnitude of fluid exchange necessary for the vortex–vortex rebound:

$$S_{ex} \propto \Delta = \sqrt{\Delta_x^2 + \Delta_y^2} \propto \sqrt{(u_f - u_i)^2 + (v_f - v_i)^2}. \tag{54}$$

The subscript i (f) of the velocity components in (54) refers to the time period before (after) the collision.

To test our rebound model, we performed a series of experiments in which we systematically varied the initial *y*-offset of the vortices ($Y_0(0)$), while keeping other parameters fixed. Figure 7 presents examples of the vorticity patterns realized immediately after the rebound. For each experiment, we recorded the amount of fluid exchanged during the collision (S_{ex}), as well as the change in the eddy propagation velocity ($|\delta V|$). Overall, the numerical $S_{ex}(|\delta V|)$ dependence (figure 8) is consistent with the predicted linear relation (54), which supports our view of the inviscid rebound as a consequence of fluid exchange between colliding vortices. We note a small uniform offset in $S_{ex}(\delta V)$ for low values of $|\delta V|$, which we attribute to the remote interaction effects: even for non-colliding eddies ($S_{ex} = 0$) there is a small change in velocity ($\delta V \neq 0$).
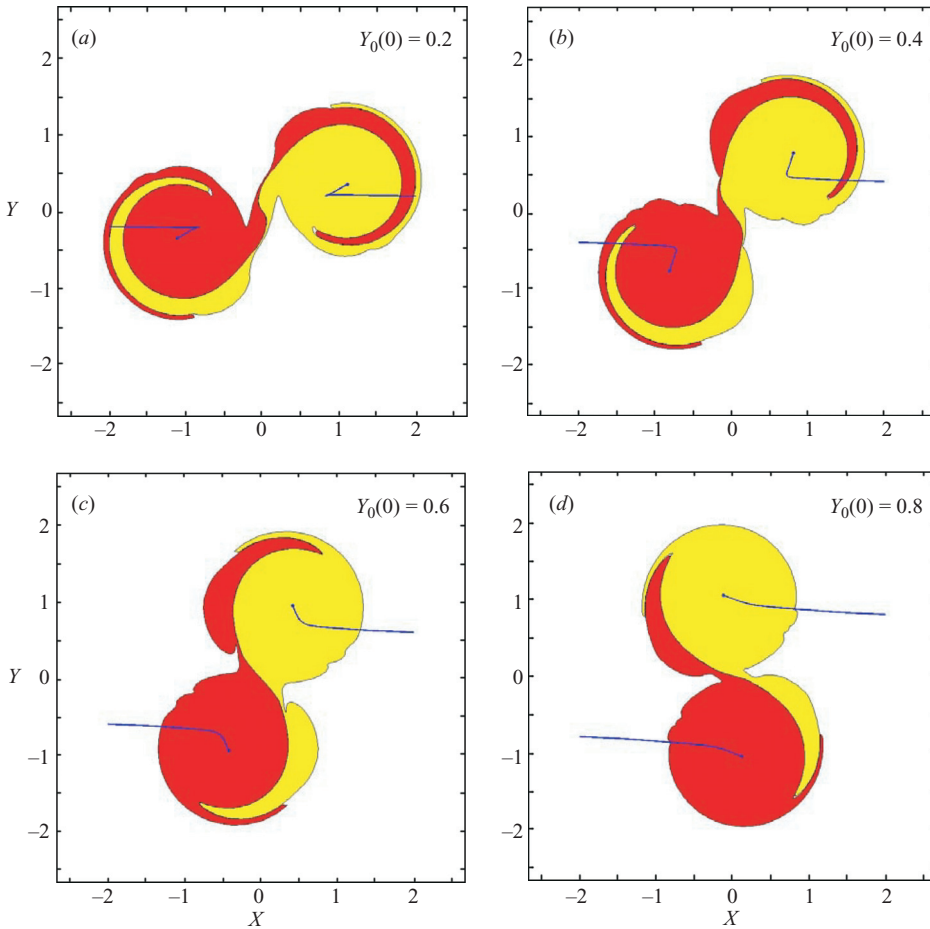
FIGURE 7. Examples of colliding eddies. In the numerical experiments we used $X_C(0) = X_0(0) = 2$, $Y_C(0) = Y_0(0) - 0.1$, and various values of $Y_0(0)$. Presented are the vorticity patterns immediately after the rebound.
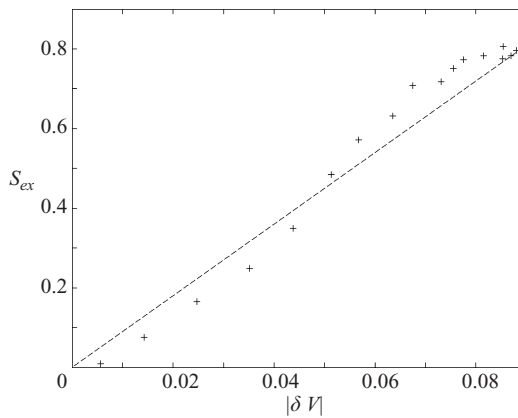

FIGURE 8. For each experiment with colliding eddies, we plot the amount of fluid exchanged during the collision (S_{ex}) as a function of the variation in eddy propagation velocity ($|\delta V|$). The data points (plus signs) conform to the predicted linear relation (54). The best fit of the data and theory (dashed line) suggests $S_{ex} \approx 9|\delta V|$.

Before completing the discussion of two isolated vortices, we wish to emphasize two very pronounced characteristics of eddy–eddy collisions, evident in all our simulations (figure 7): (i) collisions are largely elastic – they do not lead to significant changes in the absolute value of the propagation velocity, and (ii) the angle of incidence of colliding vortices, relative to the line connecting the vortex centres at the moment of collision, is close to the angle of reflection. While the first effect can be rationalized by the principle of energy conservation†, the second one, symmetric refraction of eddies, requires a more elaborate explanation. Our interpretation is based on the conservation of angular momentum principle (e.g. Saffman 1992) – a global invariant of the two-dimensional inviscid motion:

$$\frac{\mathrm{d}}{\mathrm{d}t} \iint \frac{1}{2}(x^2 + y^2)\varsigma \, \mathrm{d}x \, \mathrm{d}y = 0. \tag{55}$$

Since the two interacting eddies in our model (figure 1b) are identical, their contributions to the total angular momentum are equal and therefore (55) can be applied to each eddy separately. Equation (55) further simplifies for vortices that are sufficiently separated from each other $\rho_0 = \sqrt{X_0^2 + Y_0^2} \gg 1$ (i.e. long before or long after the collision). In this case the angular momentum reduces, at the leading order in ρ_0^{-1}, to

$$I = \iint \frac{1}{2}(x^2 + y^2)\varsigma \, \mathrm{d}x \, \mathrm{d}y \approx X_0 \iint x\varsigma \, \mathrm{d}x\mathrm{d}y + Y_0 \iint x\varsigma \, \mathrm{d}x\mathrm{d}y$$
$$= \rho_0(Q_x \cos \gamma + Q_y \sin \gamma). \tag{56}$$

In polar coordinates (ρ, γ), such that $\rho = \sqrt{x^2 + y^2}$ and $\gamma = \arg(x + iy)$, the combination $Q_\rho = Q_x \cos \gamma + Q_y \sin \gamma$ in (56) represents the radial component of the dipolar moment. Recalling that the eddy dipolar moment is directly related to its propagation velocity (§2), we express the angular momentum (I) in terms of the eddy azimuthal velocity component (V_γ) and its separation from the origin of the coordinate system (ρ_0):

$$I = -2\pi \rho_0 V_\gamma. \tag{57}$$

Since I is an invariant, as is the absolute value of the total velocity, we conclude that the vortex collisions tend to preserve the azimuthal component of the propagation velocity $V_\gamma(\rho_0)$ but reverse its radial component, which rationalizes the observed symmetry of the refraction of colliding eddies.

6. Conclusions and suggestions

This study examines the long-range interactions and direct collisions of two shielded vortices using numerical calculations and weakly nonlinear theory.

Because of the assumption of zero net vorticity, the propagation and interaction of vortices in our model are entirely due to their initial dipolar components. These weak dipoles, masked by the dominant axisymmetric circulations, force the interaction and are modified in the process. We demonstrate that the direct eddy collisions

---

† The total energy of the propagating eddies consists of two major components – the energy associated with the axisymmetric rotation and the energy of self-propagation. If the total energy is preserved, and if the rotational energy, which in our model is determined by the vortex dimensions, also does not change, then the energy associated with vortex propagation – hence the magnitude of propagation velocity – has to be preserved as well.

are characterized by a substantial exchange of fluid between the colliding vortices, which directly affects the eddy dipolar moments and ultimately results in nearly elastic rebounds. The nonlinear dynamics of the remote vortex–vortex interactions are captured by the balanced asymptotic expansion about the basic state consisting of steady circular eddies. We derive the amplitude equations for the eddy dipolar components and use these equations to construct a low-order model of eddy evolution. We predict, and confirm numerically, that the long-range vortex–vortex interaction results in a permanent, albeit somewhat weak, change in the direction of eddy propagation.

The problem of interaction of shielded eddies appears to be much more tractable than the classical merger model, owing to the existence of a simple basic steady state in our case. Therefore, the broader significance of the proposed theoretical approach lies in the possibility of applying it to other remote interaction problems, including the interaction of shielded eddies with distant boundaries, topography, and currents. We are particularly optimistic with regard to the prospects of analytical explorations of the asymmetric configurations, consisting of two unequal sized vortices, and stratified vortex–vortex interactions.

Another line of inquiry which, so far, has been explored only to a limited extent (Carton 1992; Beckers *et al.* 2002), is related to a proposition that oceanic eddies are not shielded completely. Our present study and the classical merger models can be thought of as two extremes of the interaction problem – we emphasize the self-propagation and ignore the exterior circulation; the merger models do the opposite. It would be of interest to include both effects in a single framework and examine their cumulative effect. For instance, none of our simulations resulted in vortex mergers, whereas such phenomena are fairly common in the ocean (Cresswell 1982; Yasuda, Okuda & Hirai 1992; Flament *et al.* 2001). What is the critical merger-inducing ingredient that is missing in our idealized model? Dritschel (1986) examined a wide range of uniform distributions of vorticity, arriving at the general conclusion that the transition from one equilibrium state to another is induced by the instabilities and controlled by the integral invariants of the two states (energy and angular momentum). Both stability characteristics and global invariants are different for shielded and unshielded vortex configurations. Thus, while the merger dynamics is beyond the scope of our study, we speculate that the small but non-zero far-field circulation in the oceanic eddies could be a reason for the observed mergers.

Appendix A. Numerical experiments with vortices of different sizes

In order to ensure that the central example considered in this paper – the interaction of two identical vortices – captures some of the dynamics of the asymmetric interactions, we now present the numerical experiments with vortices of different size.

The first experiment (figure 9*b*) was initialized with two shielded circular vortices. The radius of the yellow vortex equals unity, and the radius of the red vortex is one half. Both distributed vortices have the same (unit) vorticity values, and the compensating point vortices were placed at

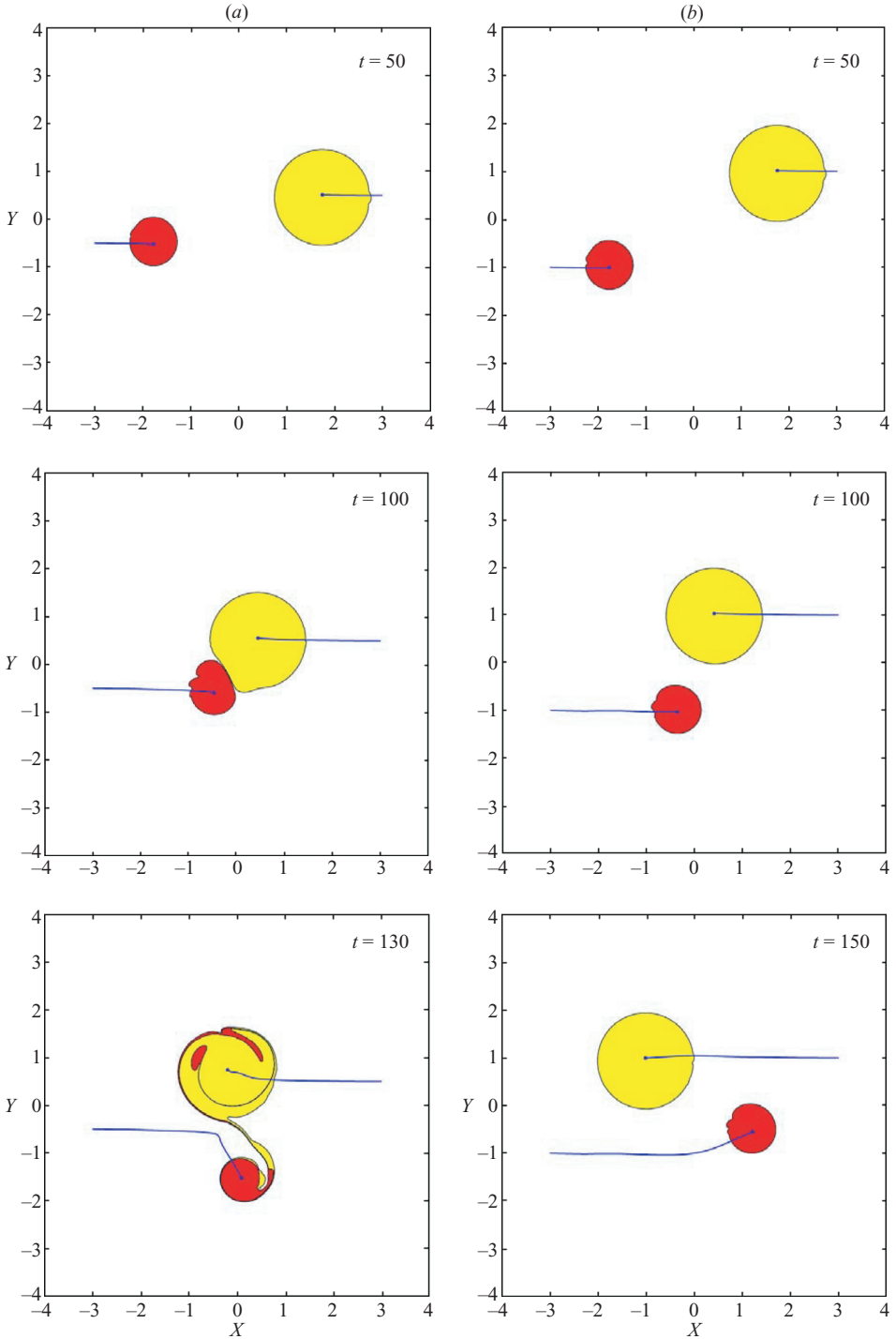$$(X_0, Y_0) = (3, 1), \quad (X_0^*, Y_0^*) = (-3, -1). \qquad (A\,1)$$

FIGURE 9. Numerical experiments with vortices of different size: (*a*) shows colliding vortice and (*b*) non-colliding. The regions of distributed vorticity are shown in red and yellow, and the blue curves represent trajectories of the point vortices. Note the permanent change in the direction of motion caused by the remote interaction of non-colliding eddies and the nearly elastic rebound accompanied by the exchange of fluid between the colliding eddies.

The centres of the vorticity contours were slightly displaced with respect to (A1) as follows:

$$X_C = X_0, \ \ Y_C = Y_0 - 0.05, \\ X_C^* = X_0^*, \ \ Y_C^* = Y_0^* + 0.05. \Big\} \tag{A 2}$$

As discussed in §2, this small y-displacement introduces a dipolar moment which propels vortices in the x-direction. This initial configuration enables the vortices to pass each other without collision. The evolutionary pattern of this system is qualitatively similar to the experiments with two identical vortices (figure 2). The first stage represents the rectilinear motion of vortices – the vortices exert only a slight influence on their partner and the trajectories are almost straight (see the configuration realized at $t = 50$ in figure 9a). This pattern of motion changes when the eddies come into close proximity. Their trajectories become visibly deflected: first, eddies make gentle right turns ($t = 100$) and then, after passing their partner, turn left ($t = 150$). The vortices do not recover their initial orientation, and the net effect of their weak encounter is to produce a finite y-velocity component – the component which was absent initially. As a result, the vortices scatter at a finite angle relative to their original direction of motion. The smaller vortex is deflected more than the larger one.

In the second experiment (figure 9a), the compensating point vortices were placed at

$$(X_0, Y_0) = (3, 0.5), \\ (X_0^*, Y_0^*) = (-3, -0.5). \Big\} \tag{A 3}$$

and their centres were displaced according to (A2). This initial orientation results in the direct collision of the propagating vortices. One again, the evolution of vortices is consistent with the strong interaction scenario, previously illustrated in figure 7. We note the nearly elastic rebound of vortices after the collision, which is accompanied by a substantial exchange of fluid.

The foregoing experiments are presented here only as preliminary evidence suggesting that the qualitative conclusions, reached by considering a special case of two identical vortices, may be sufficiently general. The problem of the asymmetric interaction is characterized by a much wider parameter space and holds the promise of rich dynamics. Thus, we propose that the vortex theory would benefit from future systematic explorations, numerical and analytical, of the asymmetric shielded eddy–eddy interactions.

Appendix B. Linear stability analysis for a system of two isolated vortices

Linear stability of the axisymmetric isolated vortex has been explored in detail by Michalke & Timme (1967) and by Flierl (1988). In these models, the circular inner core of uniform vorticity was surrounded by a compensating annulus of different (but also uniform) vorticity, with no circulation outside the eddy. It was demonstrated that the barotropic vortex (Michalke & Timme 1967) is linearly stable as long as the annulus is sufficiently wide: the radius of the inner contour is less than the half-radius of the outer contour. This result implies that eddies used in our model – the point anticyclonic vortex in a circular cyclonic vorticity patch – are individually stable. It remains to be determined whether the two-vortex configurations are stable as well. For that, the displacement of the vorticity interface of the first vortex $R = 1 + \Delta R(\theta)$

is decomposed into Fourier harmonics:

$$\Delta R(\theta) = \sum_{m=1}^{\infty} A_m \cos(m\theta) + B_m \sin(m\theta). \tag{B1}$$

As previously, the interacting vortices are symmetric, as implied in (22).

We now linearize the governing equations with respect to $(A_m, B_m) \ll 1$, in which case the kinematic condition (24) reduces to

$$\frac{\partial R}{\partial t} = U \cos\theta + V \sin\theta \tag{B2}$$

where $\boldsymbol{V}(\theta) = (U, V)$ are the material velocities of particles at the boundary of the distributed vorticity patch relative to the point vortex. The linearization of the velocity equations (§ 3.1) is written as follows:

$$U \approx L_U(\Delta R), \quad V \approx L_V(\Delta R), \tag{B3}$$

where L_U and L_V are the linear operators acting on the perturbation of the vorticity contour relative to the unit circle. The linear response (L_{Um}, L_{Vm}) is computed for each Fourier harmonic in (B1): for $m = 1$ we obtain

$$\left.\begin{aligned} L_{U1} &= -\frac{A_1 \sin(2\theta)}{2} + \frac{B_1 \cos(2\theta)}{2} - \frac{B_1}{2} + \frac{A_1 \sin\theta + B_1 \cos\theta}{l^3}, \\ L_{V1} &= \frac{A_1 \cos(2\theta)}{2} + \frac{A_1}{2} + \frac{B_1 \sin(2\theta)}{2} + \frac{A_1 \cos\theta - B_1 \sin\theta}{l^3}, \end{aligned}\right\} \tag{B4}$$

whereas for $m > 1$

$$\left.\begin{aligned} L_{Um} &= -\frac{A_m}{2} \sin(m\theta + \theta) + \frac{B_m}{2} \cos(m\theta + \theta), \\ L_{Vm} &= \frac{A_m}{2} \cos(m\theta + \theta) + \frac{B_m}{2} \sin(m\theta + \theta). \end{aligned}\right\} \tag{B5}$$

The linear velocity operators L_U and L_V are combined into a single operator for the contour displacement L_R using (B2), and the following linear response for each Fourier harmonic is obtained:

$$\left.\begin{aligned} L_{Rm} &= \frac{A_1 \sin(2\theta) + B_1 \cos(2\theta)}{l^3} && \text{for } m = 1, \\ L_{Rm} &= -\frac{A_m}{2} \sin(m\theta) + \frac{B_m}{2} \cos(m\theta) && \text{for } m > 1. \end{aligned}\right\} \tag{B6}$$

Note that the linear operator L_R does not produce the first Fourier harmonic – the eddy dipolar component. This feature is a key element of the nonlinear theory in § 3: the inability of the linear operator to generate the $m = 1$ harmonic was exploited in formulating a solvability condition at the second (nonlinear) order of expansion.

In terms of (A_m, B_m), the evolutionary equation (B2) becomes

$$\left.\begin{aligned} &\frac{\partial A_1}{\partial t} = 0, \quad \frac{\partial B_1}{\partial t} = 0, \\ &\frac{\partial A_2}{\partial t} = \frac{B_1}{l^3} + \frac{B_2}{2}, \quad \frac{\partial B_2}{\partial t} = \frac{A_1}{l^3} - \frac{A_2}{2}, \\ &\frac{\partial A_m}{\partial t} = \frac{B_m}{2}, \quad \frac{\partial B_m}{\partial t} = -\frac{A_m}{2} \quad \text{for } m > 2, \end{aligned}\right\} \tag{B7}$$

which we write in the matrix form by introducing the complex Fourier amplitudes $C_m = A_m + iB_m$. Defining a state vector

$$\mathbf{Z} = \begin{pmatrix} A_1 \\ B_1 \\ C_2 \\ C_3 \\ \ldots \\ C_n \end{pmatrix}, \tag{B 8}$$

reduces (B7) to

$$\frac{\partial}{\partial t}\mathbf{Z} = \mathbf{M}\cdot\mathbf{Z}, \tag{B 9}$$

where

$$\mathbf{M} = \begin{pmatrix} 0 & 0 & 0 & 0 & \ldots \\ 0 & 0 & 0 & 0 & \ldots \\ il^{-3} & l^{-3} & -i/2 & 0 & \ldots \\ 0 & 0 & 0 & -i/2 & \ldots \\ & & \ldots & & \end{pmatrix}. \tag{B 10}$$

This matrix has two eigenvalues: $\lambda = -i/2$, corresponding to the angular rotation of $m > 1$ modes, and $\lambda = 0$ of the degenerate dipolar ($m = 1$) mode. Since neither of those reflects the exponential growth of perturbations, we conclude that the two-vortex configuration is linearly stable.

REFERENCES

ADEM, J. 1956 A series solution for the barotropic vorticity equation and its application in the study of atmospheric vortices. *Tellus* **8**, 364–372.

BECKERS, M., CLERCX, H. J. H., VAN HEIJST, G. J. F. & VERZICCO, R. 2002 Dipole formation by two interacting shielded monopoles in a stratified fluid. *Phys. Fluids* **14**, 704–720.

BECKERS, M., VERZICCO, R., CLERCX, H. J. H. & VAN HEIJST, G. J. F. 2001 'Dynamics of pancake-like vortices in a stratified fluid: experiments, model and numerical simulations. *J. Fluid Mech.* **433**, 1–27.

CARTON, X. J. 1992 On the merger of shielded vortices. *Europhys. Lett.* **18**, 697–703.

CARTON, X. J. 2001 Hydrodynamical modeling of oceanic vortices. *Surveys Geophys.* **22**, 179–263.

CHASSIGNET, E. P., OLSON, D. B. & BOUDRA, D. B. 1990 Motion and evolution of oceanic rings in a numerical model and in observations. *J. Geophys. Res.* **95**, 22121–22140.

CHRISTIANSEN, J. P. & ZABUSKY, N. J. 1973 Instability, coalescence and fission of finite-area vortex structures. *J. Fluid Mech.* **61**, 219–243.

CORNILLON, P. & PARK, K. A. 2001 Warm core ring velocities inferred from NSCAT. *Geophys. Res. Lett.* **28**, 575–578.

CRESSWELL, G. R. 1982 The coalescence of two East Australia Current warm-core rings. *Science* **215**, 161–164.

DRITSCHEL, G. 1986 The non-linear evolution of rotating configurations of uniform vorticity. *J. Fluid Mech.* **172**, 157–182.

FLAMENT, P., LUMPKIN, R. TOURNADRE, J. & ARMI, L. 2001 Vortex pairing in an unstable anticyclonic shear flow: Discrete subharmonics of one pendulum day. *J. Fluid Mech.* **440**, 401–409.

FLIERL, G. R. 1988 On the instability of geostrophic vortices. *J. Fluid Mech.* **197**, 349–388.

GRIFFITHS, R. W. & HOPFINGER, E. J. 1986 Experiments with baroclinic vortex pairs in a rotating fluid. *J. Fluid Mech.* **173**, 501–518.

GRIFFITHS, R. W. & HOPFINGER, E. J. 1987 Coalescing of geostrophic vortices. *J. Fluid Mech.* **178**, 73–97.

Hogg, N. G. & Stommel, H. M. 1985 The heton, an elementary interaction between discrete baroclinic geostrophic vortices and its implications concerning eddy heat-flow. *Proc. R. Soc. Lond.* A **397**, 1–20.

Joyce, T. M. & McDougall, T. J. 1992 Physical structure and temporal evolution of Gulf Stream warm-core ring 82B. *Deep-Sea Res.* A **39**, S19–S44.

Killworth, P. D. 1986 On the propagation of isolated multilayer and continuously stratified eddies. *J. Phys. Oceanogr.* **16**, 709–716.

McWilliams, J. C. 1984 The emergence of isolated coherent vortices in turbulent flow. *J. Fluid Mech.* **146**, 21–43.

McWilliams, J. C. & Flierl, G. R. 1979 On the evolution of isolated, nonlinear vortices. *J. Phys. Oceanogr.* **9**, 1155–1182.

Melander, M. V., Zabusky, N. J. & McWilliams, J. C. 1988 Symmetric vortex merger in two dimensions: Causes and conditions. *J. Fluid Mech.* **195**, 303–340.

Michalke, A. & Timme A. 1967 On the inviscid stability of certain two-dimensional vortex-type flows. *J. Fluid Mech.* **29**, 647–666.

Nof, D. 1981 On the beta-induced movement of isolated baroclinic eddies. *J. Phys. Oceanogr.* **11**, 1662–1672.

Nof, D. 1983 On the migration of isolated eddies with application to Gulf Stream rings. *J. Mar. Res.* **41**, 399–425.

Olson, D. B. 1980 The physical oceanography of two rings observed by the cyclonic ring experiment. Part II: Dynamics. *J. Phys. Oceanogr.* **10**, 514–528.

Olson, D. B. 1991 Rings in the ocean. *Annu. Rev. Earth Planet. Sci.* **19**, 283–311.

Olson, D. B., Schmitt, R. W., Kennelly, M. & Joyce, T. M. 1985 A two-layer diagnostic model of the long-term physical evolution of warm-core ring 82B. *J. Geophys. Res.* **90**, 8813–8822.

Radko, T. & Stern, M. E. 1999 On the propagation of oceanic mesoscale vortices. *J. Fluid Mech.* **380**, 39–57.

Radko, T. & Stern, M. E. 2000 Self-propagating eddies on the stratifed f-plane. *J. Phys. Oceanogr.* **30**, 3134–3144.

Robinson, A. R. (Ed.) 1983 *Eddies in Marine Science.* Springer.

Saffman, P. G. 1992 *Vortex Dynamics.* Cambridge University Press.

Stern, M. E. 1987 Horizontal entrainment and detrainment in large-scale eddies. *J. Phys. Oceanogr.* **17**, 1688–1695.

Stern, M. E. 2000 Scattering of an eddy advected by a current towards a topographic obstacle. *J. Fluid Mech.* **402**, 211–223.

Stern, M. E. & Pratt, L. J. 1985 Dynamics of vorticity fronts. *J. Fluid Mech.* **161**, 513–532.

Stern, M. E. & Radko, T. 1998 The self propagating quasi-monopolar vortex. *J. Phys. Oceanogr.* **28**, 22–39.

Sutyrin, G. G. & Flierl, G. R. 1994 Intense vortex motion on the beta plane: development of the beta gyres. *J. Atmos. Sci.* **51**, 773–790.

Trieling, R. R. & van Heijst, G. J. F. 1998 Decay of monopolar vortices in a stratified fluid. *Fluid Dyn. Res.* **23**, 27–43.

Yasuda, I. & Flierl, G. R. 1995 Two-dimensional asymmetric vortex merger: contour dynamics experiment. *J. Oceanogr.* **51**, 145–170.

Yasuda, I., Okuda K. & Hirai, M. 1992 Evolution of a Kuroshi warm-core ring: Variability of the hydrographic structure. *Deep-Sea Res.* 39 (Suppl.), 5131–5161.

Zabusky N. J., Hughes, M. H. & Roberts K. V. 1979 Contour dynamics for the Euler equations in two dimensions. *J. Comput. Phys.* **30**, 96–106.